energy&fuels

pubs.acs.org/EF Article

Model Lignin Oligomer Pyrolysis: Coupled Conformational and Thermodynamic Analysis of β-O-4′ Bond Cleavage

Tanzina Azad, Jonathan D. Schuler, Maria L. Auad, Thomas Elder, and Andrew J. Adamczyk*

Cite This: https://dx.doi.org/10.1021/acs.energyfuels.0c01573 Read Online

ACCESS | Metrics & More | Article Recommendations | Supporting Information

ABSTRACT: The abundance, carbon content, and functionalized nature of lignin make it a promising candidate for targeted valorization to fuels and polymer composites. While lignin modeling by the application of computational chemistry is an active area of research, electronic structure methods have been limited mainly to structures in the dimeric or trimeric range. In this study, we have modeled a lignin structure composed of 10 β-O-4′ linked guaiacyl (G) units, such that this work represents, to the best of our knowledge, the largest structure that has been examined to date using quantum mechanical calculations. As such, this work can provide information on a model, the size of which is more representative of the lignin polymer than has been previously reported. We have calculated bond dissociation enthalpy (BDE) for the homolytic cleavage reaction between each G unit in our model lignin oligomer, which occurs as one of the initial reactions during lignin pyrolysis. The objective of the current work was to determine how or if reactivity within the oligomer changes as a function of bond cleaving position within the chain. The methods used were classical molecular mechanics for conformational sampling and quantum mechanically based density functional theory (DFT) calculations. We have developed a novel and robust method for conformational sampling, which maps the conformational energy landscape efficiently and provides multiple low-energy structures that are then used to determine the BDE values by DFT. Our results for BDE calculations of lignin exhibit significant position dependence along the oligomer chain. To the best of our knowledge, we have reported for the first time the calculated standard thermodynamic properties including enthalpy of formation, heat capacity, entropy, and Gibbs free energy. Despite using a simplified model lignin oligomer structure, our calculated values for standard thermodynamic properties have a remarkable agreement with the experimental values.

INTRODUCTION

Among the three polymers that form plant cell walls (i.e., cellulose, lignin, and hemicellulose), lignin is the second most abundant natural polymer. Lignin provides reinforcement to the cell walls, contributes to water interactions, and serves as a physical barrier to pathogens.[1] As a biopolymer, it accounts for 30% of the organic carbon content in the biosphere.[2] The biosynthesis of lignin can be divided into three processes, biosynthesis of lignin monomers followed by their transportation and polymerization.[3] Lignin monomers are produced in the cytoplasm of plant cell, transported to the apoplast, and finally polymerized by peroxidase (POD) and laccase (LAC) enzymes in the secondary cell wall.[4,5] Depending on the plant species, lignin constitutes 12−28% of the total lignocellulosic biomass, where the other two components are cellulose (30−40%) and hemicellulose (24−38%).[6] Despite the fact that current knowledge of lignin structure is far from complete, according to the current understanding, lignin is a hydrophobic polymer composed of phenyl propanoid units, resulting from the oxidative polymerization of the *para*-hydroxy coumaryl alcohol, coniferyl alcohol, and sinapyl alcohol.[7] The proportion of each of these cinnamyl alcohols incorporated into the polymer varies widely with species. In addition to the canonical cinnamyl alcohols, recent work has found that other phenolics function as lignin monomers that can serve as nucleation sites or occur within the polymer itself.[8−12] The first step in lignin polymerization is an enzymatic dehydrogenation resulting in phenoxy radicals, in which there is considerable delocalization of the unpaired electrons. As the coupling process proceeds, there are numerous reactive sites resulting in diverse linkage types, which is shown in Table 1. Among these, the most common is the β-O-4′, which is the subject of our study.[13]

Fast pyrolysis is the process of thermal degradation at elevated temperatures in the absence of oxygen for short reactor residence time. The subsequent condensation of these pyrolysis vapors yields a complex liquid mixture of organic compounds, commonly referred to as bio-oil.[16−18] Pyrolysis-based technologies are promising for converting lignocellulosic biomass into biochemicals, biomaterials, and biofuels.[19−23] However, to control and optimize these processes in an efficient way to ensure higher product yield and selectivity, a better understanding of basic lignin structure as the input and associated thermodynamic and kinetic parameters is important.[24−26] The chemical mechanisms associated with these processes of lignin have been studied both experimentally and computationally.[27−32] Due to the irregular structure and recalcitrant nature of lignin, lignin pyrolysis reactions are not straightforward.[33−35]

Received: May 16, 2020
Revised: July 13, 2020
Published: July 14, 2020

https://dx.doi.org/10.1021/acs.energyfuels.0c01573
Energy Fuels XXXX, XXX, XXX−XXX

Table 1. Diverse Linkage Types Found in Lignin and Their Relative Amount[14,15]

Linkage Type	Structures	Relative Abundance
β-O-4′	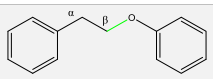	50-60%
β-5	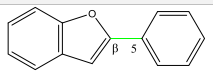	6-11%
5-5	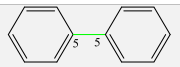	5-12%
α-O-4	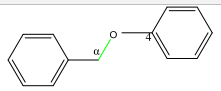	5-7%
4-O-5	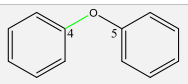	4-7%
β- β	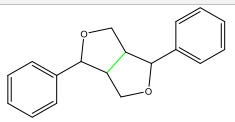	2-6%
β-1	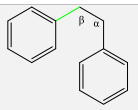	1-2%

Therefore, such studies are conducted with model compounds with specifically chosen interunit linkages. It has also been reported that the initial step in lignin pyrolysis[36] is a homolytic bond cleavage. This reaction has been the subject of extensive quantum-based theoretical studies.[37−42] However, due to the computational intensity, such work has mainly been limited to dimers and trimers. Both concerted and homolytic cleavage mechanisms have been proposed to occur in the initial steps of lignin pyrolysis. The activation energy of the Maccoll elimination reaction is found to be somewhat lower than the bond dissociation energy of homolytic cleavage.[38] It has also been found that the homolytic reaction is dominant at higher temperatures.[43] Neither of these papers shows that the homolytic cleavage reaction does not occur. As such, and so that comparisons can be made with the extensive literature on homolytic cleavage of dimers, this work was focused on the homolysis reaction. While there are considerable computational results for bond dissociation enthalpy (BDE) of the β-O-4′ linkage using smaller lignin structures, larger oligomers, more representative of the polymer itself, have not been addressed.

The lignin model used in this study is a simplified structure representing a relatively low-molecular-weight oligomer with a single interunit linkage. Models of this type, composed exclusively of β-O-4′ linkages, have been prepared synthetically[44,45] and been the subject of NMR[46] and thermal analyses[47] and as such have precedent in the experimental literature. The current paper applies computational methods to such structures. The natural lignin polymer is much more complex with varying interunit linkages; however, one of the key objectives of this work is concerned with isolating the effect of the position within the oligomer on bond dissociation enthalpies. If differing interunit linkages had been used, it would have been impossible to systematically separate the effects of position and bond type. Furthermore, while there have been extensive studies on bond dissociation of lignin dimers, to the best of our knowledge, this is the first time that a lignin model of this size has been examined using electronic structure methods. As such, this work can provide information on a model, the size of which is more representative of the lignin polymer than has been previously reported.

Contemporary computational methods have been applied to evaluate the reaction enthalpies, electronic structure, and optimized geometries associated with a guaiacyl 10-mer oligolignol connected through β-O-4′ linakges, which occurs as one of the initial reactions during lignin pyrolysis. Given the possible flexibility of such an oligomer, classical molecular mechanics (MM) has been used for performing conformational sampling in this study. Though the literature on conformational sampling for lignin is not as extensive as for proteins, there are considerable amounts of molecular dynamics (MD) research works done on lignin.[48−52] Though the reliability of molecular mechanics (MM) energies depends on the parameterization of the respective force field, rarely force fields have been specifically parameterized for lignin.[53,54] We have developed a novel and robust method for lignin oligomer conformational sampling, which maps the conformational energy landscape efficiently and provides multiple low-energy structures using a stochastic Monte Carlo (MC) algorithm. Furthermore, we have constructed a lignin conformer library, which is a product of the conformational sampling method, which could be very useful for further computational studies and cross validation with experiments. Subsequently, density functional theory (DFT) and statistical thermodynamics calculations have been used for the determination of BDE for the lowest-energy conformers identified in the previous step. Finally, the thermochemical properties by way of enthalpy, entropy, free energy, and constant pressure heat capacity values were estimated using conventional statistical thermodynamics formulas. Predicted values for BDE and the thermodynamic properties were found to be in reasonable agreement with the available experimental and literature values for lignin structures of diverse origins.

COMPUTATIONAL METHODOLOGY

Reaction Pathway Schemes. The structure under consideration in the current work, as shown in Figure 1a, is a 10-mer of G units linked through β-O-4′ bonds. While this is a highly idealized structure, in order to address the objective concerned with determining whether BDE changes as a function of position within the oligomer, the inclusion of a more realistic linkage pattern would have confounded the problem by introducing the additional variable of linkage type and position within the oligomer. It should be noted, however, that such structures are not without precedent and have been produced synthetically.[44−46] The initial structure was developed using the Lignin Builder algorithm[55] which randomly assigns stereochemistry to chiral centers. This approximation is necessitated by the presence of 18 chiral centers, which translates into 262,144 possible stereoisomers, an examination of which would be an obviously intractable problem. The reactions that were examined for this structure are shown in Table 2, representing sequential homolytic cleavage of each β-O-4′ bond to determine if and how reactivity varies with position. While, as indicated, there is considerable literature related to the application of electronic structure methods to various dimeric and trimeric lignin models, to the best of our knowledge such calculations have not been attempted for larger oligomers, and until the

https://dx.doi.org/10.1021/acs.energyfuels.0c01573
Energy Fuels XXXX, XXX, XXX−XXX

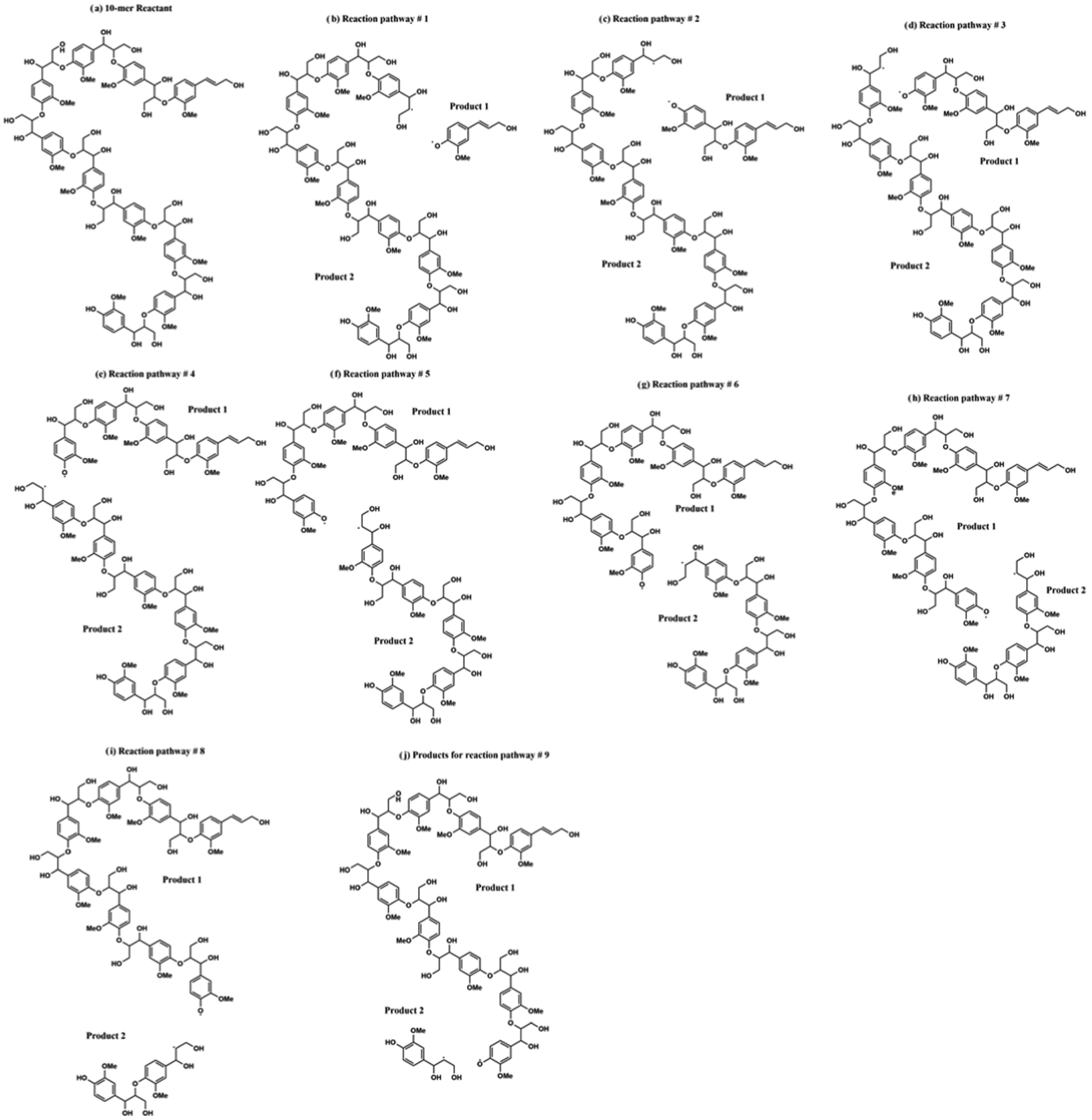

Figure 1. (a) Initial reactant structure; (b–j) two radical products obtained along each of the nine reaction schemes for studying β-O-4′ BDE. Products 1 and 2 are radical fragments with the radical center on the oxygen and secondary carbon atoms, respectively, after β-O-4′ bond cleavage.

current study, it was unknown if BDE differs between the individual G units in a larger structure.

Conformational Analysis. Conformational sampling using molecular mechanics (MM) calculations is a very common approach that is performed prior to quantum chemical calculations, especially for macromolecular systems, such as (bio)polymers. Therefore, in this study, MM has been used as an essential step to refine the input structures for DFT calculations. The results of any classical molecular modeling calculations, including conformational sampling, depend largely on the choice of the force field. Different force fields have specific priorities, e.g., a large coverage of elements (UFF),[56] emphasis on the quality of structure prediction (AMBER,[57] CHARMM[58]), and emphasis on high accuracy in predicting various molecular properties with a fairly broad coverage (COMPASS),[59] which has been used in this work. COMPASS is based on the PCFF, which is one of the first force fields developed for polymers. To improve the nonbonded interaction terms, PCFF had been reparameterized and as a result, COMPASS has been developed by employing a hybrid approach consisting of both *ab initio* and empirical methods. The functional forms used in COMPASS are given by

https://dx.doi.org/10.1021/acs.energyfuels.0c01573
Energy Fuels XXXX, XXX, XXX−XXX

Table 2. Reaction Schemes for Studying Position Dependence of β-O-4′ BDE in a Model Lignin Oligomer[a]

Reactant	Reaction pathway	Product 1	Product 2
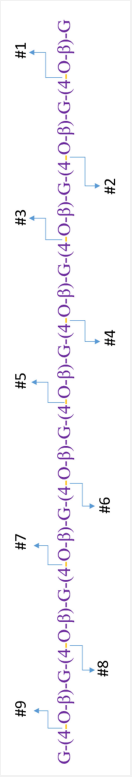	1	·O-β-G	G-(4-O-β)-G-(4-O-β)-G-(4-O-β)-G-(4-O-β)-G-(4-O-β)-G-(4-O-β)-G-(4-O-β)-G-4·
	2	·O-β-G-(4-O-β)-G	G-(4-O-β)-G-(4-O-β)-G-(4-O-β)-G-(4-O-β)-G-(4-O-β)-G-(4-O-β)-G-4·
	3	·O-β-G-(4-O-β)-G-(4-O-β)-G	G-(4-O-β)-G-(4-O-β)-G-(4-O-β)-G-(4-O-β)-G-(4-O-β)-G-4·
	4	·O-β-G-(4-O-β)-G-(4-O-β)-G-(4-O-β)-G	G-(4-O-β)-G-(4-O-β)-G-(4-O-β)-G-(4-O-β)-G-4 ·
	5	·O-β-G-(4-O-β)-G-(4-O-β)-G-(4-O-β)-G-(4-O-β)-G	G-(4-O-β)-G-(4-O-β)-G-(4-O-β)-G-(4-O-β)-G-4·
	6	·O-β-G-(4-O-β)-G-(4-O-β)-G-(4-O-β)-G-(4-O-β)-G-(4-O-β)-G	G-(4-O-β)-G-(4-O-β)-G-(4-O-β)-G-4·
	7	·O-β-G-(4-O-β)-G-(4-O-β)-G-(4-O-β)-G-(4-O-β)-G-(4-O-β)-G-(4-O-β)-G	G-(4-O-β)-G-(4-O-β)-G-4·
	8	·O-β-G-(4-O-β)-G-(4-O-β)-G-(4-O-β)-G-(4-O-β)-G-(4-O-β)-G-(4-O-β)-G-(4-O-β)-G	G-(4-O-β)-G-4·
	9	·O-β-G-(4-O-β)-G-(4-O-β)-G-(4-O-β)-G-(4-O-β)-G-(4-O-β)-G-(4-O-β)-G-(4-O-β)-G-(4-O-β)-G	G-4·

[a]The reaction pathways and oligomer sequences follow the notation introduced in Figure 1.

$$E_{\text{total}} = \sum_{b} [k_2(b - b_0)^2 + k_3(b - b_0)^3 + k_4(b - b_0)^4] + \sum_{\theta} [k_2(\theta - \theta_0)^2 + k_3(\theta - \theta_0)^3 + k_4(\theta - \theta_0)^4]$$
$$+ \sum_{\phi} [k_1(1 - \cos\phi) + k_2(1 - \cos 2\phi) + k_3(1 - \cos 3\phi)] + \sum_{\chi} k_2\chi^2 + \sum_{b,b'} k(b - b_0)(b' - b_0') + \sum_{b,\theta} k(b - b_0)(\theta - \theta_0)$$
$$+ \sum_{b,\phi} (b - b_0)[k_1 \cos\phi + k_2 \cos 2\phi + k_3 \cos 3\phi] + \sum_{\theta,\phi} (\theta - \theta_0)[k_1 \cos\phi + k_2 \cos 2\phi + k_3 \cos 3\phi] + \sum_{\theta,b} k(\theta - \theta_0)(\theta' - \theta_0')$$
$$+ \sum_{\theta,\theta',\phi} k(\theta - \theta_0)(\theta' - \theta_0')\cos\phi + \sum_{i,j} \frac{q_i q_j}{r_{ij}} + \sum_{i,j} \epsilon_{ij}\left[2\left(\frac{r_{ij}^0}{r_{ij}}\right)^9 - 3\left(\frac{r_{ij}^0}{r_{ij}}\right)^6\right] \quad (1)$$

where the valence terms represent the internal coordinates of bond (b), angle (θ), torsion angle (ϕ), and out-of-plane angle (χ). The Lennard-Jones parameters are denoted by ϵ_{ij} and r_{ij0}, while q_i denotes the partial charge and k denotes a constant particular to an element. The cross-coupling terms combine two or three internal coordinates, which are important for predicting vibrational frequencies and structural variations associated with conformational changes.

Given the large number of rotatable bonds, or dihedral angles capable of torsion, in the model being used, a stochastic conformational search was performed by the application of the Boltzmann jump method, which uses the Metropolis Monte Carlo (MC) criterion to accept or reject a jump in structural change due to torsional displacement.[60] To determine the value for the variables in the energy expression used for total energy calculation in COMPASS, we performed a rigorous sensitivity analysis which includes, temperature, torsional angle window, and the number of perturbations per jump as the major variables. Our chosen value for the torsion angle window and the number of perturbations per jump were 10° and 50 perturbations per jump, respectively. Our study indicates that the required value for temperature is a function of structure size. The COMPASS force field was used for all calculations in this study. All of the bonds in the structure capable of torsion were rotated stochastically in the allowed torsion angle window of 10° and the energy was calculated for each interval. Electrostatic and van

https://dx.doi.org/10.1021/acs.energyfuels.0c01573
Energy Fuels XXXX, XXX, XXX−XXX

der Waals (vdW) summation methods were atom-based and performed with cubic spline truncation, a cutoff distance of 12.5 Å, a spline width of 1 Å, and a buffer width of 0.5 Å. In our semiautomated sampling method, the lowest-energy structure from each conformational search step was selected as the input structure for the next step in an iterative manner. The process is repeated until no statistically significant change in end-to-end distance is found between the initial and final structures. The number of conformational search steps has been found to vary as a function of structure size, increasing proportionally with structure size. Geometry optimization using classical MM was performed for each structure during this conformation sampling.

Among the major parameters used for this sampling method, sampling temperature associated with the Metropolis MC selection criterion[60] has been found to play an important role. In this study, the temperature effect on sampling has been studied for a wide range starting from 273 to 50,000 K. It has been found that an optimum temperature is needed for all structures as sampling is performed, where the requirement of optimum temperatures selection depends on the structure size. The optimum sampling temperatures are not physical. The high temperatures are used to include more energy in the system to overcome conformational sampling time scales. That is, these high temperatures were needed to provide the energy to change the dihedral angles with a relatively high probability for the Metropolis MC selection criterion. This dependency has been shown in Table 3.

Table 3. Dependence of Required Temperature on the Structure Size for the Developed Conformational Sampling Method Based on the Metropolis Monte Carlo (MC) Selection Criterion[60a]

structure size	nonphysical optimum temperature (K) for conformational sampling method based on metropolis Monte Carlo (MC) selection criterion
1−4-mer	5000
5−7-mer	25 000
8−10-mer	50 000

[a]Temperature values reported in units of kelvin, but the sampling temperatures are not physical.

It should be noted that this sampling method has used the COMPASS force field, which has been carefully parameterized for synthetic phenolic polymers with and without cross-linking.[61] These phenolic polymers closely resemble the structure of naturally occurring lignin. The structures obtained using our developed sampling method and the COMPASS force field are then used as an input to higher-level quantum chemical calculations and statistical thermodynamics. Given the reasonable parameterization for synthetic phenolic polymers, we found the COMPASS force field to be acceptable for application to lignin oligomers as the geometry inputs to the electronic structure calculations converged successfully with minimal self-consistent field (SCF) cycles and geometry steps. We are not guaranteed to have found the global minimum for the lignin 10-mer or fragments, rather a novel conformational sampling method was developed to improve our input structure to the DFT calculation providing a local energy minimum. Together, the conformational sampling, DFT calculations, and application statistical thermodynamics comprise our composite method presented herein, which has been validated against the computational and experimental thermochemical properties from the literature in the Results and Discussion section.

Electronic Structure Calculations. For the DFT calculations in this study, all electrons were included for each atom without the use of pseudopotentials, and the BLYP functional, DNP numerical basis set, and 4.4 Å global orbital cutoff energy were employed. A numerical basis set of double-zeta quality plus polarization functions (DNP) was chosen because it provides more computationally feasible and similarly accurate calculations for macromolecules than its numerical equivalent Gaussian basis set, 6-31G**. All electronic energies were carried out using quantum chemical calculations with the density functional theory in the Dmol3 package.[62,63] The generalized gradient approximation (GGA) with Becke−Lee−Yang−Parr (BLYP) was selected as the exchange−correlation functional.[64] We had implemented the B3LYP (Becke, 3-parameter, Lee−Yang−Parr) hybrid exchange−correlation functional, which is more commonly used in the literature,[65] but the B3LYP functional was not practical beyond a 4-mer given computational resource constraints. To describe the London dispersion force interaction appropriately, the Tkatchenko−Scheffler (TS) method was used for DFT-D correction.[66] For all structures including products and reactants, only the lowest-energy conformer was used for geometry optimization at the BLYP-DNP level, where the convergence criteria were set as 2×10^{-5} Hartrees (Ha) for total energy, 0.004 Ha/Å for the maximum force of every atom, and 0.005 Å for maximum displacement. The self-consistent-field (SCF) tolerance was set to be 1×10^{-5} Ha. Compounds that are smaller in size and inorganic in nature having similar reactive features to this work have been extensively studied with success previously in our group using comparable hybrid methodologies.[67−72] The accuracy of the BLYP/DNP level of theory has been documented for the reaction energetics and thermochemistry of similar organic and biopolymers.[73−76]

Statistical Thermodynamics. Vibrational frequency calculations of these optimized structures were performed to determine the thermochemical parameters: enthalpy (H), entropy (S), free energy (G), and heat capacity at constant pressure (C_p). These values reported in this work are based on the standard statistical thermodynamic calculations using the standard molecular partition functions of polyatomic gas molecules.[77] It is important to mention that the thermochemical properties are calculated using quantum chemical calculations and statistical thermodynamics. Statistical thermodynamics requires the calculation of a molecular partition function, which has electronic, rotational, vibrational, and translational contributions. Different conformations of the lignin fragments will affect these contributions and thus result in different molecular partition functions as a result of conformation. These variations in conformation would manifest through a change in the molecular properties, e.g., bond angle strain, which may change the electron density around β-O-4′ linkages or different moments of inertia if the fragments deviated from the spherical shape. The enthalpy correction, H, using the ideal gas approximation is given by eq 2

$$H(T) = E_{vib}(T) + E_{rot}(T) + E_{trans}(T) + RT \quad (2)$$

where the subscripts represent vibrational, rotational, and translational contributions, respectively, and R is the ideal gas constant. The contributions are given by

https://dx.doi.org/10.1021/acs.energyfuels.0c01573
Energy Fuels XXXX, XXX, XXX−XXX

$$E_{trans} = \frac{3}{2}RT \tag{2.1}$$

$$E_{rot(linear)} = RT \tag{2.2}$$

$$E_{rot(nonlinear)} = \frac{3}{2}RT \tag{2.3}$$

$$E_{vib} = \frac{R}{k}\frac{1}{2}\sum_i h\nu_i + \frac{R}{k}\sum_i \frac{h\nu_i \exp(-\frac{h\nu_i}{kT})}{[1-\exp(-\frac{h\nu_i}{kT})]} \tag{2.4}$$

where k and h are the Boltzmann and Planck's constants, respectively, and ν_i is the individual vibrational frequency.

Similarly, heat capacity at constant pressure (C_p) calculations are based on the ideal gas approximation and is given by eq 3

$$C_p(T) = C_{p,vib}(T) + C_{p,rot}(T) + C_{p,trans}(T) + RT \tag{3}$$

The contributions are given by

$$C_{p,trans} = \frac{5}{2}RT \tag{3.1}$$

$$C_{p,rot(linear)} = R \tag{3.2}$$

$$C_{p,rot(nonlinear)} = \frac{3}{2}RT \tag{3.3}$$

$$C_{p,vib} = R\sum_i \frac{\left(\frac{h\nu_i}{kT}\right)^2 \exp(-\frac{h\nu_i}{kT})}{\left[1-\exp\left(-\frac{h\nu_i}{kT}\right)\right]^2} \tag{3.4}$$

The entropy correction is given by eq 4

$$S(T) = S_{vib}(T) + S_{rot}(T) + S_{trans}(T) + RT \tag{4}$$

The contributions are given by

$$S_{trans} = \frac{5}{2}R\ln T + \frac{3}{2}R\ln\omega - R\ln p - 2.31482 \tag{4.1}$$

$$S_{rot(linear)} = R\ln\frac{8\prod^2 IkT}{\sigma h^2} + R \tag{4.2}$$

$$S_{rot(nonlinear)} = \frac{R}{2}\ln\left[\frac{\prod}{\sqrt{\sigma}}\frac{8\prod^2 cI_A}{h}\frac{8\prod^2 cI_B}{h}\frac{8\prod^2 cI_C}{h}\left(\frac{Tk_B}{hc}\right)^3\right] + \frac{3}{2}R \tag{4.3}$$

$$S_{vib} = R\sum_i \frac{\frac{h\nu_i}{k_BT}\exp\left(-\frac{h\nu_i}{k_BT}\right)}{1-\exp\left(-\frac{h\nu_i}{k_BT}\right)} - R\sum_i \ln\left[1-\exp\left(-\frac{h\nu_i}{k_BT}\right)\right] \tag{4.4}$$

where ω denotes the molecular weight, I_x is the moment of inertia about axis x, and σ is the rotational symmetry number.

Bond Dissociation Enthalpies. Bond dissociation enthalpies were calculated as the difference of the sum of the standard enthalpies of formation of the product fragments and the standard enthalpy of formation of the reactant, as shown in eq 5

$$BDE_{298\ (reactant)} = [\Delta H^\circ_{f,298\ (product\ 1)} + \Delta H^\circ_{f,298\ (product\ 2)}] - \Delta H^\circ_{f,298\ (reactant)} \tag{5}$$

where $\Delta H^\circ_{f,298}$ is the standard enthalpy of formation of the radical species products 1 and 2 and the 10-mer lignin molecule as the reactant. These standard enthalpy of formation values are calculated using a hybrid methodology based on quantum chemical calculations, statistical thermodynamics, and experimental atomization energies as performed in previous work from our group.[67]

The basis for these standard enthalpy of formation values was calculated using eqs 2, 2.1.2.1−2.4.2.4 to account for the enthalpy correction, then this correction was added to the electronic energy (E_{el}) and zero point energies (ZPE) using eq 6

$$H_{298} = E_{el} + ZPE + H(T) \tag{6}$$

The standard enthalpy of formation of a given species ($C_xH_yO_z$) was then calculated from its atomization energy using eq 7

$$\Delta H^\circ_{f,298}(C_xH_yO_z) = [x\Delta H^\circ_{f,298}(C) + y\Delta H^\circ_{f,298}(H) + z\Delta H^\circ_{f,298}(O)] - \Delta H^\circ_{a,298}(C_xH_yO_z) \tag{7}$$

where the enthalpies of formation of atomic C, H, and O are the experimental values obtained from the NIST-JANAF thermochemical tables ($\Delta H^\circ_{f,298}(C)$ = 172.001 kcal mol^{-1}, $\Delta H^\circ_{f,298}(H)$ = 52.32 kcal mol^{-1}, and $\Delta H^\circ_{f,298}(O)$ = 59.803 kcal mol^{-1}) and $\Delta H^\circ_{a,298}(C_xH_yO_z)$ is the atomization enthalpy defined as the enthalpy change upon decomposition of a molecule into its component atoms, which can be evaluated as eq 7.1.7.1

$$\Delta H^\circ_{a,298}(C_xH_yO_z) = [xH_{298}(C) + yH_{298}(H) + zH_{298}(O)] - H_{298}(C_xH_yO_z) \tag{7.1}$$

where $H_{298}(C)$, $H_{298}(H)$, and $H_{298}(O)$ are the enthalpies of atomic C, H, and O at 298 K, respectively, and $H_{298}(C_xH_yO_z)$ is the enthalpy of $C_xH_yO_z$ at the same temperature. These enthalpies can be calculated as previously mentioned in eqs 2, 2.1.2.1−2.4.2.4, 6. These quantities are obtained from quantum chemical calculations and statistical thermodynamics.

The enthalpy of reaction at the elevated temperature, or BDE at temperature T, is then calculated using the calculated BDE_{298K} and the temperature-dependent heat capacity values following eq 8

$$BDE_T = BDE_{298K} + \int_{298K}^{T} \Delta C_{P,Rxn}(T)\,dT \tag{8}$$

where $\Delta C_{p,Rxn}(T)$ is the temperature-dependent polynomial defined as the difference between the sum of temperature-dependent standard heat capacities of the products and the temperature-dependent standard heat capacity of the reactant.

RESULTS AND DISCUSSION

Conformational Analysis. The conformational analysis of the model lignin structures of this study suggests two key findings: (i) the rearrangement does not depend on the starting conformation, as the same folding with energy minimization was observed for the all starting compounds, radical or closed shell, and the starting conformation (helical) is not conserved in the rearranged 10-mer reactant and product fragments; (ii) no regioselectivity was observed in the case of radical containing fragments, oxygen or carbon radical, indicating that the main driving force is the decrease of the external surface area of the macromolecule and increase in the number of intramolecular interactions, including but not limited to hydrogen bonding and $\pi-\pi$ bond interaction between unsaturated benzene rings, irrespective of the β-O-4′ bond position being cleaved. Here, the

https://dx.doi.org/10.1021/acs.energyfuels.0c01573
Energy Fuels XXXX, XXX, XXX−XXX

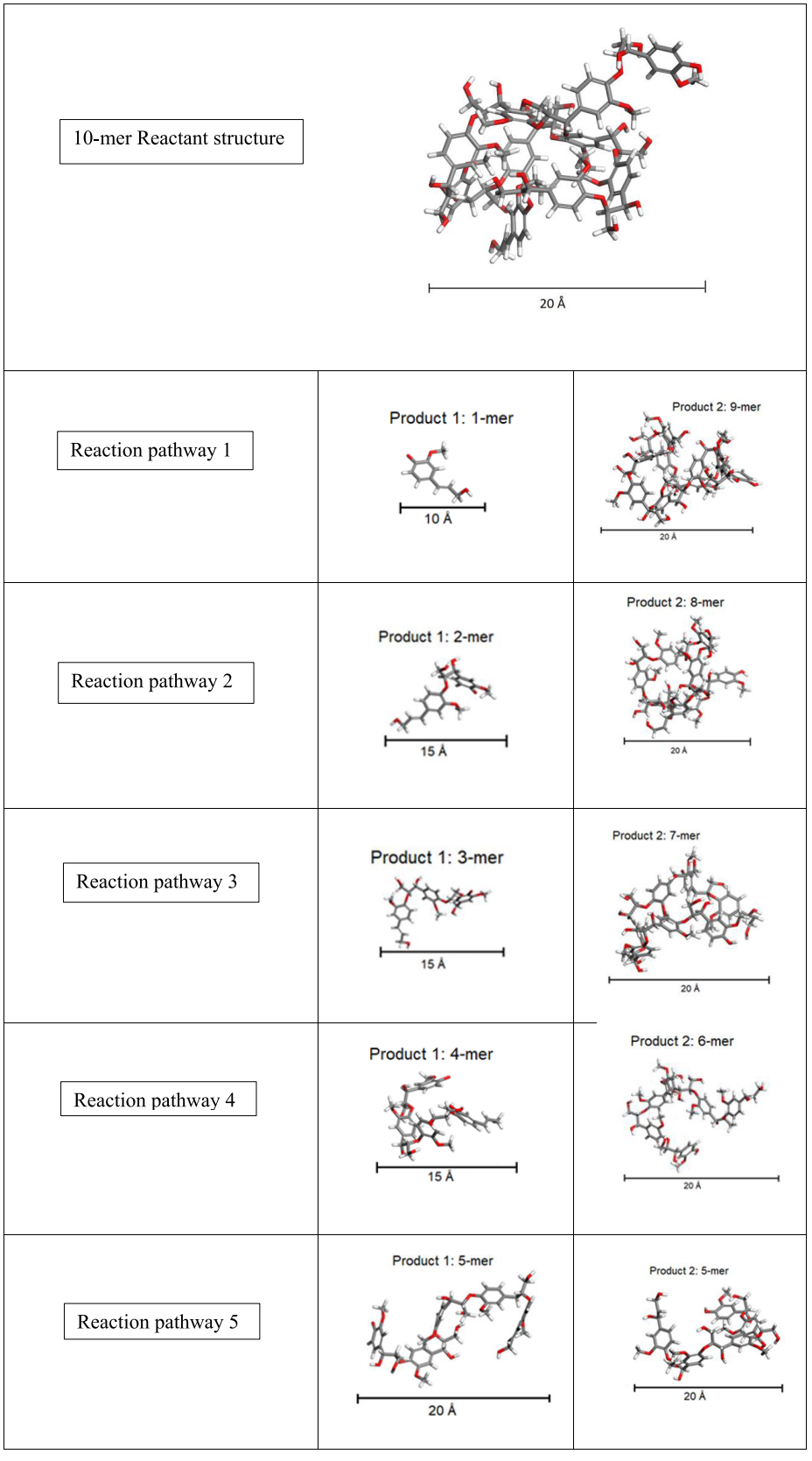

Figure 2. continued

https://dx.doi.org/10.1021/acs.energyfuels.0c01573
Energy Fuels XXXX, XXX, XXX−XXX

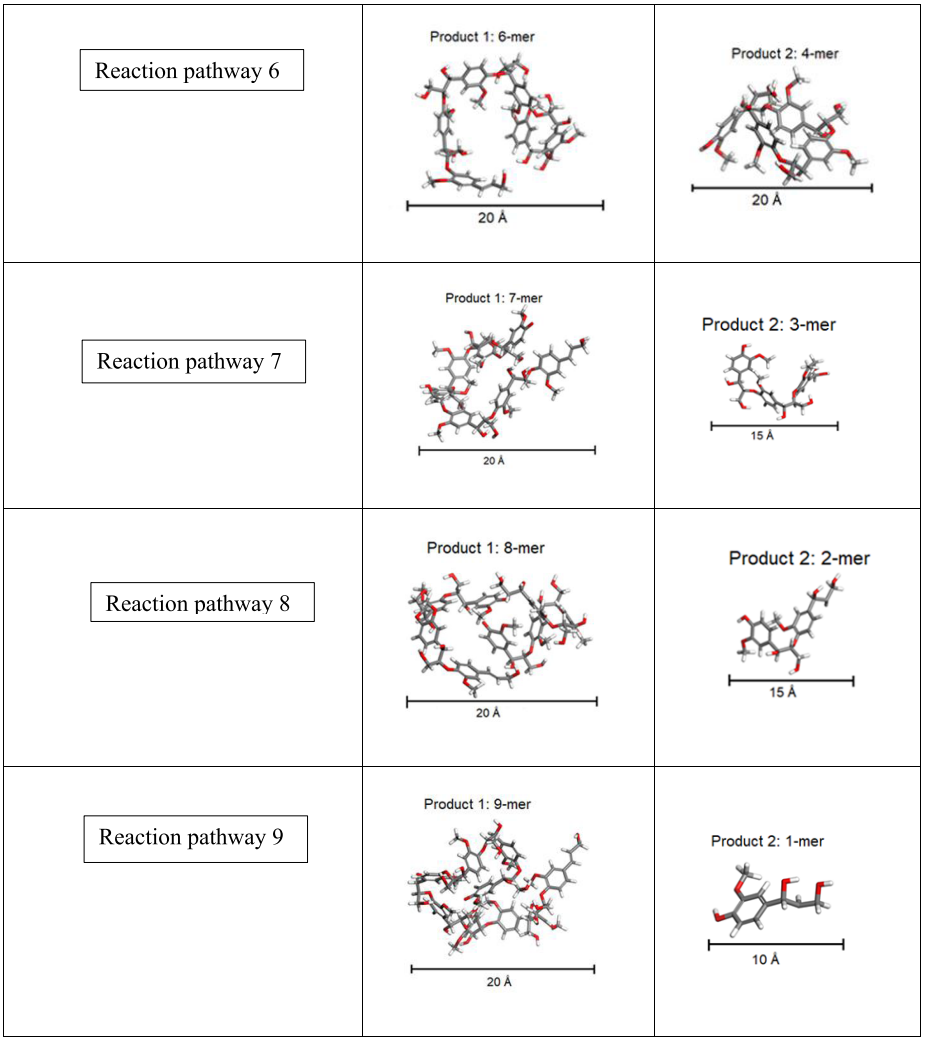

Figure 2. Optimized structures for all products and the reactant at the BLYP/DNP level of theory. The two products of the homolysis of the β-O-4′ bond are phenoxy radical and C free radical, which are denoted by product 1 and 2, respectively. Reaction products for the nine reaction pathways are shown.

lack of regioselectivity refers to no reaction selectivity trend observed between the β-O-4′ bond cleavage position and the stereochemistry of the cleaved product fragments.

We have considered end-to-end distance measurement, which is a characteristic length for a polymer. In polymers such as lignin, end-to-end distance is measured between the two end points in the polymer chain. By performing conformational sampling, the initial model oligomer structure, which was unfolded (initial end-to-end distance 42 Å), has been significantly folded (25 Å). This folding of structures occurs as a result of total energy reduction in systems by structural change. Folding of structures, in other words, results in a reduction in energy of the structures and increased with the increase in chain length, which can be clearly seen in Figure 2. The end-to-end distance values of these folded structures have been reported in Table 4.

Conformational Landscape. As the output of this conformational sampling method, a large library of lignin conformers has been generated, which can be used as a database of lignin model structures, ranging from monomer to 10-mer with different dihedral angles and different MM energies. It should be noted that only a systematic grid scan could ensure the identification of the global minima, which has not been used in this work. For example, in the 10-mer reactant molecule, a total of 57 dihedral angles were stochastically sampled to map the conformation landscape of the oligomers in this study and only these 57 dihedral angles were varied to select the different conformers. In principle, it would be more accurate if all dihedral angles could be varied systematically and all of the lowest-energy conformations on the conformational landscape could be

Table 4. End-to-End Distance Obtained in the Lowest-Energy Structure for Each Species after Conformational Sampling

reaction pathway	product 1 structures	end-to-end distance (Å)	product 2 structures	end-to-end distance (Å)
1	1-mer	8.7	9-mer	11.1
2	2-mer	11.6	8-mer	19.7
3	3-mer	17.8	7-mer	12.1
4	4-mer	9.0	6-mer	20.8
5	5-mer	21.4	5-mer	12.5
6	6-mer	15.1	4-mer	8.9
7	7-mer	9.5	3-mer	12.5
8	8-mer	10.8	2-mer	12.4
9	9-mer	16.4	1-mer	5.1
reactant	10-mer	25.7		

https://dx.doi.org/10.1021/acs.energyfuels.0c01573
Energy Fuels XXXX, XXX, XXX−XXX

studied with DFT for BDE analysis. However, extensive calculations on a number of these 10-mer structures may prove interesting for statistical analysis, but it is beyond the scope of this study.

Bond Dissociation Enthalpies. As previously mentioned, determining whether or not reaction enthalpy varies with the position of the β-O-4′ bond along the model lignin oligomer chain was the major objective of this work. Table 5 shows the value of reaction enthalpy of each pathway followed in this study. The elementary reaction step for β-O-4′ bond cleavage studied is intended to be the same for all of the nine pathways, and each cleavage originates from the same lowest-energy 10-mer conformation. The lack of conservation of the starting conformation after cleavage could be explained by considering the need to stabilize the exposed radical center, oxygen or carbon, after homolytic bond cleavage. As conformational change initiates after bond cleavage, the unsaturated phenolic rings rearrange to maximize $\pi-\pi$ stacking and hydrogen bonding and the interaction of the generated radical center with electron-rich functionalities is maximized.

Table 5. Bond Dissociation Enthalpy Values for Each Reaction Pathway Studied to Examine the Position Dependence of Homolytic β-O-4′ Bond Cleavage in a Model 10-mer Oligomer of Lignin

reaction pathway	calculated BDEs values for 25−1000 K (kcal mol^{-1})	BDE value at 298 K (kcal mol^{-1})
1	63.9−64.9	64.4
2	46.8−62.6	50.1
3	64.6−66.0	65.4
4	54.4−52.8	54.4
5	59.4−67.6	62.1
6	61.9−64.8	63.0
7	67.9−77.2	69.6
8	56.4−59.0	57.5
9	57.0−67.1	59.3

In the Conformation Analysis section, it was highlighted that an output of our conformational sampling method is a large library of lignin conformers. The BDE value for this process can also be estimated from the helical structure before energy minimization, similar to lignin 10-mer dissolved in a suitable solvent such as tetrahydrofuran (THF), dimethyl sulfoxide (DMSO), and dimethylformamide (DMF), where the lignin aromatic system is exposed and it is nearly free to interact with other solvent molecules thereby maximizing the solvent-exposed surface area. Although beyond the scope of this study, it is likely that ring flipping (torsion) happens faster than lignin macromolecule folding in the solvent phase; however, in the gas-phase for our study, both conformational motions appear competitive, particularly at elevated temperatures under pyrolysis. The unfolded starting structure (open, helical) could also serve as an estimation of the limit of the BDE, which minimizes the role of intramolecular interactions. Details regarding the unfolded starting structure for the model 10-mer oligomer of lignin are available in the Supporting Information.

Factors Contributing to the Stability of Radicals. For the study of the homolytic C−H bond cleavage, it has been shown that alkyl radicals tend to have a BDE value of 93.6−105.6 kcal mol^{-1}, whereas arylic radicals have been reported to have BDE values in the order of 110.4−136.8 kcal mol^{-1}.[78−80] In our study, product 1 species are phenoxy radicals, while product 2 species are secondary carbon free-radical structures having both alkyl and arylic functionalities. Product 2 free-radical species exhibit medium stability being secondary free radical in nature. On the other hand, product 1 structures are phenoxy radicals, which are stabilized by resonance throughout the conjugated system of connected π orbitals with delocalized electrons in the nearby aromatic ring functionality. Since BDE values reflect the stability of these radical products from β-O-4′ bond cleavage, our calculations indicate that at the reference temperature 298.15 K, the radical species formed in pathway 2 are the most stable radicals, while the least stable radical species have been observed in pathway 7. For pathway 7, analysis indicates that higher nonbonded energy contributions for the phenoxy radical product structure are the primary reason for the outlier behavior. This is a consequence of the observed variation of the BDE value with β-O-4 bond cleaving position, which reveals different reaction pathways with different degrees of local and nonlocal radical stabilization effects.

Our study reveals distinct thermodynamic differences in the homolytic cleavage reaction at different points in the oligomer. For all nine reaction pathways that have been studied here, enthalpies of the β-O-4′ bond cleavage reaction showed distinguishable position dependence. Not all, but for some reactions, the reaction enthalpies showed temperature dependence as well. Between these two effects, the position effect is more dominant than the temperature effect for the range of temperatures relevant to pyrolysis presented here. Reaction enthalpies calculated over the entire temperature range considered in this study have been listed in the Supporting Information. Figure 3 shows the position dependence of our calculated BDE at the primary pyrolysis temperature range of lignin (300−400 °C).

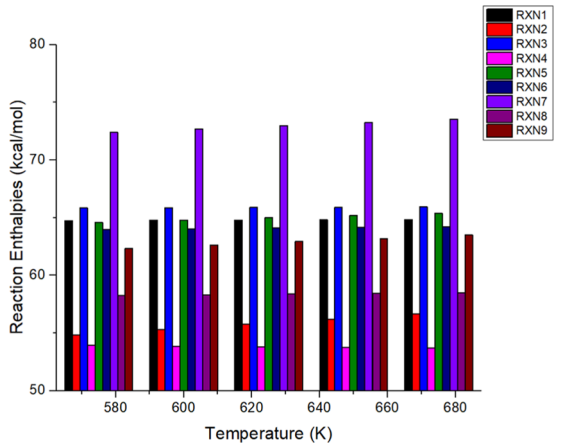

Figure 3. Bond dissociation enthalpy values for β-O-4′ cleavage reaction in model lignin oligomer at different positions under the primary pyrolysis temperature range.

Table 6 lists some of the recent BDE studies for the β-O-4′ linkage using model lignin structures. It is notable that DFT is the preferred method and the Minnesota functional M06-2X has been widely used. Among the basis sets, 6-31++G(2df,p) is one of the largest basis set that has been used to study the model lignin dimer. In our study, we used BLYP functional for affordable computational cost of the large 10-mer structure of lignin; however, our primary results of BDE values at nine different cleavage positions in model oligomer are well within the range of BDE values predicted using the other DFT method

https://dx.doi.org/10.1021/acs.energyfuels.0c01573
Energy Fuels XXXX, XXX, XXX−XXX

Table 6. Bond Dissociation Enthalpy (BDE) Values for β-O-4′ Cleavage Reaction from the Literature

Structure	Method	BDE (kcal mol^{-1})	References
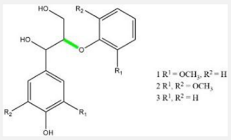	DFT (B3LYP/6-31++G(2df,p))	54.5	79
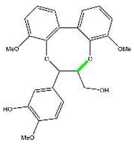	DFT (M06-2X/6-31+G(d) for Geometry Optimization, 6-311++G(d,p) for Vibrational Frequencies	57.1	36
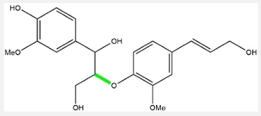	DFT (M06-2X/6-311++G(d,p) for Geometry Optimization and Vibrational Frequencies	68.8	38
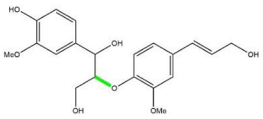	Composite Method (Semi-empirical PM6 Hamiltonian for Geometry optimization, re-optimization with M06-2X/6-31G(d), M06-2X/6-311++G(d,p))	69.2	42
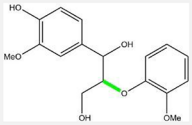	DFT (M06-2X/6-311++G(d,p)	67.3	41
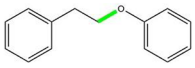	DFT (B3LYP/6-31G(d,p) for Geometry Optimization, 6-31++G(d,p) for Vibrational Frequencies	61.5	39
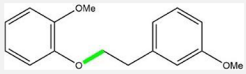	DFT (M06-2X/6-31+G(d,p)	65.8	80

in the literature. Our study reveals that the BLYP functional and basis set of double-zeta quality plus polarization functions can be used to successfully predict BDE values for β-O-4′ bond cleavage studies in significantly larger oligomers while ensuring comparable accuracy to the higher levels of theory used for smaller dimer structures.

For reaction 1, the enthalpy of reaction varied from 63.9 to 64.9 kcal mol^{-1} over the temperature range 25−1000 K. In terms of the product sizes, reaction 9 is similar, but the reaction enthalpy varied from 57.0 to 67.0 kcal mol^{-1} over the complete temperature range. This clearly shows that reaction 9 yields different reaction enthalpies at different temperatures, which was not observed for reaction pathway 1. Similar temperature dependence (about 10 kcal mol^{-1} reaction enthalpy variation as the temperature is varied) has been found for reaction 7. In reaction 7, the reaction enthalpy varied from 67.9 to 77.2 kcal mol^{-1}. Reaction 5 showed a similar temperature dependence (about 8.2 kcal mol^{-1}) with 59.4 kcal mol^{-1} at 25 K and 67.6 kcal mol^{-1} at 1000 K. The largest temperature dependence has been found in reaction 2 with a reaction enthalpy variation of 15.8 kcal mol^{-1} for the overall temperature range with 46.8 kcal mol^{-1} at 25 K and 62.6 kcal mol^{-1} at 1000 K. Reactions 1, 3, 4, 6, and 8 do not exhibit such temperature dependence. For the overall temperature range, reaction enthalpy variations were found to be 1.1, 1.4, 1.7, 3.0, 2.6 kcal mol^{-1} for reaction pathways 1, 3, 4, 6, and 8, respectively. An increasing trend of endothermicity with increasing temperature has been observed in the reactions that showed notable temperature dependence (2, 5, 7, and 9), which are shown in Figure 3. However, the reactions showing no such significant dependence also yield a slightly increasing trend of endothermicity, with the only exception being reaction 4, where

https://dx.doi.org/10.1021/acs.energyfuels.0c01573
Energy Fuels XXXX, XXX, XXX−XXX

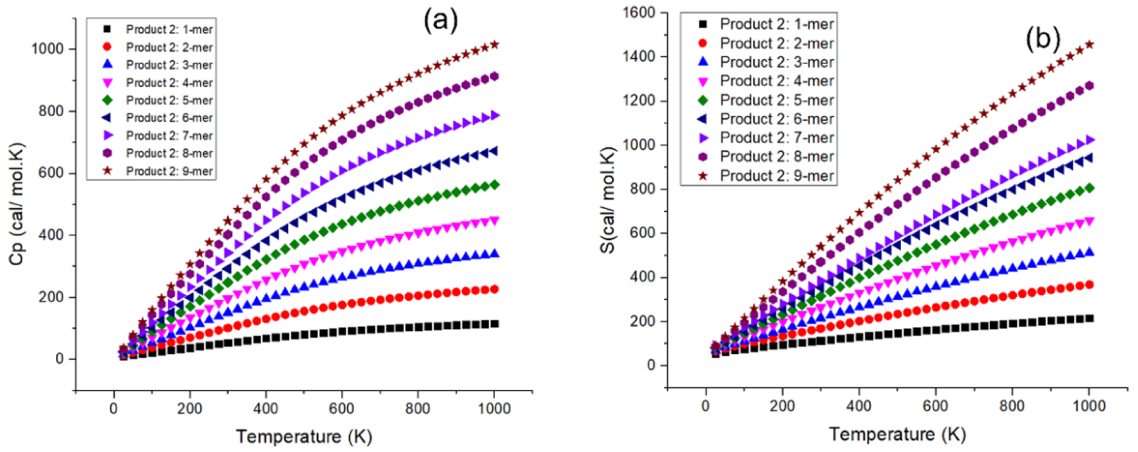

Figure 4. (a) Selected constant pressure heat capacity and (b) entropy values as a function of temperature for nine structures of product 2 (secondary carbon free-radical species). The tabulated properties at elevated temperatures for all species in this study are available in the Supporting Information.

endothermicity slightly decreased by 1.7 kcal mol^{-1} over the full temperature range.

Our results reveal a strong position dependence in BDE for β-O-4′ bond cleavage along the 10-mer lignin model oligomer structure. The observed position dependence of BDE value along the entire length of the model oligomer may depend highly on conformational sampling, which is probable due to the large number of dihedral angles capable of rotation in the system under consideration. It should be noted that our stochastic method for seeking the lowest-energy conformer cannot guarantee the identification of the global minimum on the conformer landscape for the oligomers of various sizes in this study. For the purposes of this work, the local minima identified through conformational searching were used as input structures for quantum calculations. In principle, we could sample for a large amount of time to get a more or less continuous distribution of structures from which the lowest-energy conformer could be selected with more certainty, this was however is beyond the scope of this paper. Instead, we have developed a composite QM/MM method where we have introduced cutoff criteria so that all structures could be treated with the same methodology, ensuring the highest chance of reproducibility. Due to the extremely high computational cost, higher levels of theory through the use of functionals that account for electron exchange and correlation more completely and larger basis sets have not been used in this study. However, this study indicates that the BLYP/DNP level of theory may instead be quite reasonable to study reaction enthalpy of bond cleavage reactions in larger lignin model structures. The results of BDE for β-O-4′ bond cleavage reaction of the closest model structure that matches with the dimer of our study has been reported as 69.2 kcal mol^{-1} that used the M06-2X/6-31G(d) level of theory.[81] Due to the use of different functionals and type of basis sets, as well as the type of model structures, it is not a fair comparison to our results; however, it is noteworthy to highlight that this BDE value is within the range of BDE values predicted in our study.

While the majority of the presented BDE values are within one standard deviation, it should be noted that the bond dissociation enthalpies generally differ by >1 kcal mol^{-1}, which has been defined as "chemical accuracy".[82] Structures with energies that differ by greater than chemical accuracy are considered to be thermodynamically distinct. Also, it should be emphasized that we determined a range of BDE values. Before this study, only single values of BDE have been reported as the previous models were all dimers. Since we have gone beyond dimers, we found a range of BDE values. Furthermore, the β-O-4′ homolytic cleavage reactions have been proposed to be barrierless, and as such, the activation energies can be approximated by the reaction energy.[43,83] Thus, even a 1 kcal mol^{-1} difference in E_A will lead to factor difference in rate coefficients due to exponential dependence of the Arrhenius equation on E_A. This propagation of the BDE range would affect kinetic (or reactor) modeling efforts of fast pyrolysis significantly where the purpose of the modeling efforts is aimed to control product selectivity and yield.

Standard Thermodynamic Properties. Standard thermodynamic quantities are crucial parameters for chemical engineering applications including reactor modeling and kinetic modeling. For instance, reaction enthalpy over a temperature range requires C_p values across that temperature range. During lignin pyrolysis, it is essential to know reaction enthalpy for a range of temperatures since this process occurs not at a single temperature, but over a range, particularly for larger reactors where temperature gradients are unavoidable. Fast pyrolysis technology offers certain advantages for converting lignin into valorized products such as bio-oil; however, the lack of a reactor or kinetic model that can reliably predict bio-oil molecular composition from a complex lignin feedstock is a challenge to be overcome and still an active area of research investigations.[84]

In addition to the calculation of reaction enthalpies, we have predicted the standard thermodynamic quantities, enthalpy of formation, heat capacity at constant pressure (C_p), entropy (S), and Gibbs free energy (G) for all radical and closed shell species in this study. Figure 4a shows the logarithmic relationship with temperature for heat capacity values for product 2 structures of varying size (secondary carbon free-radical species). Figure 4b shows the trend of variation of entropy values with temperature for the same structures. The range of C_p value variation was found to be 10.3−115.9 cal mol^{-1} K^{-1} for a monomer of product 2 structure over the temperature range of 25−1000 K. For the 9-mer, this range was found to be 39.3−1042.2 cal mol^{-1} K^{-1}. For the entropy variation, the monomer structure of product 2 showed a range of 55.3−216.6 cal mol^{-1} K^{-1} over the temperature range of 25−1000 K. The range of entropy variation was 91.3−1457.0 cal mol^{-1} K^{-1} for the same temperature range. All of the other thermodynamic quantities

https://dx.doi.org/10.1021/acs.energyfuels.0c01573
Energy Fuels XXXX, XXX, XXX−XXX

Table 7. (a) Heat Capacity for All Species in This Study for Selected Temperatures in Units of cal mol^{-1} K^{-1} and J g^{-1} K^{-1} and (b) Comparison of Average Predicted Heat Capacity Values to Experimental Values for Cuproammonium, Sulfuric, and Dioxane Lignin, respectively[a]

(a)

		C_p (cal mol^{-1} K^{-1})			C_p (J g^{-1} K^{-1})		
	molar mass	temperature (K)			temperature (K)		
structure (reaction, product number: name)	(g mol^{-1})	298	350	450	298	350	450
R1, P1: 1-mer	179	48.1	55.0	67.1	1.13	1.29	1.57
R2, P1: 2-mer	375	99.2	114.1	140.2	1.11	1.27	1.56
R3, P1: 3-mer	571	144.6	167.1	206.7	1.06	1.22	1.51
R4, P1: 4-mer	767	192.2	222.9	276.6	1.05	1.22	1.51
R5, P1: 5-mer	963	249.4	288.0	355.4	1.08	1.25	1.54
R6, P1: 6-mer	1159	292.9	339.4	420.5	1.06	1.23	1.52
R7, P1: 7-mer	1355	344.5	399.8	496.1	1.06	1.23	1.53
R8, P1: 8-mer	1551	387.8	450.4	559.6	1.05	1.21	1.51
R9, P1: 9-mer	1747	442.4	513.5	637.3	1.06	1.23	1.53
R9, P2: 1-mer	197	53.4	61.3	74.9	1.13	1.30	1.59
R8, P2: 2-mer	393	100.9	116.6	144.0	1.07	1.24	1.53
R7, P2: 3-mer	589	149.9	173.8	215.3	1.07	1.23	1.53
R6, P2: 4-mer	785	196.7	228.5	283.9	1.05	1.22	1.51
R5, P2: 5-mer	981	247.5	286.9	355.8	1.06	1.22	1.52
R4, P2: 6-mer	1177	292.2	339.8	422.7	1.04	1.21	1.50
R3, P2: 7-mer	1373	343.0	398.7	495.8	1.05	1.22	1.51
R2, P2: 8-mer	1569	401.8	466.2	578.1	1.07	1.24	1.54
R1, P2: 9-mer	1765	445.9	517.1	641.2	1.06	1.23	1.52
reactant: 10-mer	1944	485.5	563.9	700.9	1.05	1.21	1.51

(b)

	C_p (J g^{-1} K^{-1})		
temperature (K)	298	350	450
cuproammonium lignin*	1.24	1.42	NA
sulfuric lignin*	1.28	1.47	NA
dioxane lignin**	NA	1.21	1.95
model lignin (this study)	1.05	1.21	1.51

[a]* and ** denote refs 85 and 86, respectively.

for product 1 structures (phenoxy free-radical species) are reported in the Supporting Information.

Table 7a reports the constant pressure heat capacity of all species at three selected temperatures. Table 7b lists the experimental values for the constant pressure heat capacity with lignin samples extracted from rape straw by cuproammonium and sulfuric methods and the very good agreement of these experimental values with our calculated values. The conditional structural units were $C_{10}H_{11.9}O_{6.5}$ for cuproammonium lignin and $C_{10}H_{11.5}O_{3.9}$ for sulfuric lignin. These experimental heat capacity values were obtained using an adiabatic calorimeter for a relatively lower temperature range (5−370 K). In addition to showing strong agreement with these experimental values, our calculations provide heat capacity values over a higher-temperature range up to 1000 K.

Table 8 reports the values of enthalpy of formation calculated for all species analyzed in this study using eq 7 employing atomization enthalpies. With the increase in the number of monomers of which the products are composed, the values of enthalpy of formation decrease from −431.8 to −6783.8 kJ mol^{-1} for product 1 (phenoxy free-radical species). For product 2 (secondary carbon free-radical species), this range has been found to vary from −589.4 to −6920.0 kJ mol^{-1}. While the experimental enthalpy of formation for the monomer used in this study is −712.9 kJ mol^{-1}, enthalpy of formation per monomer obtained from our calculation for all species, ranging from 1-mer to 10-mer, can be seen in Table 8, with the percentage deviation given in the last column. Our calculated enthalpy of formation per monomer obtained from the 10-mer structure only differs from the experimental value by 6.9%, which is an excellent agreement given that we have chosen such a model lignin oligomer.

As mentioned earlier, the variation of standard entropy for all species of product 2 (secondary carbon free-radical species) as a function of temperature and structure size has been shown in Figure 4b. Table 9 reports the values of standard entropy for all species including the 10-mer reactant molecule and all species of product 1 (phenoxy free-radical species) analyzed in this study. Similar to our calculated values of standard enthalpy of formation per monomer reported in Table 8, the calculated values of standard entropy per monomer are reported in Table 9. With the experimental value for standard entropy per monomer of 239.8 J mol^{-1} K^{-1}, the percentage deviation of our calculated values from this experimental value has been listed in Table 9. Our calculated value for standard entropy per monomer obtained from the 10-mer structure only differs from the experimental value by 2.2%, which is a remarkable agreement. This agreement with the experimental values underlines the accuracy of our developed novel composite methodology, which uses classical molecular mechanics, Monte Carlo (MC)

https://dx.doi.org/10.1021/acs.energyfuels.0c01573
Energy Fuels XXXX, XXX, XXX−XXX

Table 8. Calculated Enthalpy of Formation Using Atomization Enthalpies for All Species and Deviation With the Experimental Enthalpy of Formation per Monomer[85]

structure (reaction, product number: name)	number of monomers	$\Delta H°_f$ (kcal mol^{-1})	$\Delta H°_f$ (kJ mol^{-1})	per monomer $\Delta H°_f$ (kJ mol^{-1})	per monomer deviation exp-calc (kJ mol^{-1})	% deviation
R1, P1: 1-mer	1	−103.2	−431.7	−431.7	−281.2	39.4
R2, P1: 2-mer	2	−264.8	−1107.8	−553.9	−159.0	22.3
R3, P1: 3-mer	3	−470.8	−1969.7	−656.6	−56.3	7.9
R4, P1: 4-mer	4	−669.9	−2802.8	−700.7	−12.2	1.7
R5, P1: 5-mer	5	−853.3	−3570.2	−714.0	1.1	−0.2
R6, P1: 6-mer	6	−1039.1	−4347.8	−724.6	11.7	−1.6
R7, P1: 7-mer	7	−1251.6	−5236.7	−748.1	35.2	−4.9
R8, P1: 8-mer	8	−1423.5	−5956.0	−744.5	31.6	−4.4
R9, P1: 9-mer	9	−1621.4	−6783.8	−753.8	40.9	−5.7
R9, P2: 1-mer	1	−140.9	−589.4	−589.4	−123.5	17.3
R8, P2: 2-mer	2	−340.5	−1424.7	−712.3	−0.6	0.1
R7, P2: 3-mer	3	−500.3	−2093.4	−697.8	−15.1	2.1
R6, P2: 4-mer	4	−719.4	−3009.8	−752.5	39.6	−5.5
R5, P2: 5-mer	5	−906.1	−3791.1	−758.2	45.3	−6.4
R4, P2: 6-mer	6	−1097.2	−4590.9	−765.1	52.2	−7.3
R3, P2: 7-mer	7	−1285.4	−5377.9	−768.3	55.4	−7.8
R2, P2: 8-mer	8	−1506.6	−6303.6	−788.0	75.1	−10.5
R1, P2: 9-mer	9	−1653.9	−6920.0	−768.9	56.0	−7.9
reactant: 10-mer	10	−1821.5	−7621.1	−762.1	49.2	−6.9
	per monomer	exp $\Delta H°_f$	−712.9 kJ mol^{-1}			

Table 9. Calculated Standard Entropy Values for All Species and Deviation with the Experimental Value for Standard Entropy per Monomer[85]

structure (reaction, product number: name)	number of monomers	$S°$ (cal mol^{-1} K^{-1})	$S°$ (J mol^{-1} K^{-1})	per monomer $S°$ (J mol^{-1} K^{-1})	per monomer deviation exp-calc (J mol^{-1} K^{-1})	% deviation
R1, P1: 1-mer	1	114.5	479.2	479.2	−239.4	−99.8
R2, P1: 2-mer	2	164.5	688.3	344.1	−104.3	−43.5
R3, P1: 3-mer	3	217.4	909.7	303.2	−63.4	−26.5
R4, P1: 4-mer	4	262.5	1098.4	274.6	−34.8	−14.5
R5, P1: 5-mer	5	334.9	1401.1	280.2	−40.4	−16.9
R6, P1: 6-mer	6	361.2	1511.1	251.9	−12.1	−5.0
R7, P1: 7-mer	7	419.3	1754.4	250.6	−10.8	−4.5
R8, P1: 8-mer	8	454.0	1899.4	237.4	2.4	1.0
R9, P1: 9-mer	9	507.1	2121.6	235.7	4.1	1.7
R9, P2: 1-mer	1	113.5	474.8	474.8	−235.0	−98.0
R8, P2: 2-mer	2	168.1	703.2	351.6	−111.8	−46.6
R7, P2: 3-mer	3	214.6	898.1	299.4	−59.6	−24.8
R6, P2: 4-mer	4	264.3	1106.0	276.5	−36.7	−15.3
R5, P2: 5-mer	5	314.3	1315.1	263.0	−23.2	−9.7
R4, P2: 6-mer	6	355.0	1485.4	247.6	−7.8	−3.2
R3, P2: 7-mer	7	383.3	1603.8	229.1	10.7	4.5
R2, P2: 8-mer	8	468.7	1961.2	245.1	−5.3	−2.2
R1, P2: 9-mer	9	538.2	2251.6	250.2	−10.4	−4.3
reactant: 10-mer	10	560.8	2346.4	234.6	5.2	2.2
	per monomer	exp $S°$	239.8 J mol^{-1} K^{-1}			

simulations, quantum chemistry, and statistical thermodynamics to predict the useful properties for engineers modeling lignin pyrolysis to produce bio-oil and related products.

CONCLUSIONS

Bond dissociation enthalpies (BDE) of a β-O-4′ linkage, which occurs as one of the initial reactions during lignin pyrolysis in a lignin model oligomer comprised of 10 guaiacyl (G) units, have been calculated over a wide range of temperature from 25 to 1000 K using density functional theory (DFT) calculations at the BLYP/DNP level of theory. As such, this work can provide information on a model, the size of which is more representative of the lignin polymer than has been previously reported. Prior to DFT calculations, a novel conformational sampling method was developed and performed using the COMPASS force field to identify lowest-energy structures for all products and the 10-mer

https://dx.doi.org/10.1021/acs.energyfuels.0c01573
Energy Fuels XXXX, XXX, XXX−XXX

reactant. This analysis required the development of a method for sampling of the large lignin oligomer, where the creation of a conformer library of lignin was a useful output of our mapping of the conformation landscape. Standard thermodynamic quantities, including enthalpy of formation, constant pressure heat capacity, entropy, and Gibbs free energy, have been predicted for all of the structures over the wide temperature range.

Calculations of the BDE values of the model oligomer show a marked difference in reaction enthalpies depending on the position along the oligomer. The wide range of temperature examined in this study for studying BDE reveals that BDE of the lignin model compound depends on the reaction temperature, but the conformation of the reactant and the radical fragment products will affect this temperature dependency greatly. The agreement of our calculated values for the standard thermodynamic properties with the available experimental values and the overall range of BDE variation with β-O-4′ bond cleaving position in our model oligomer reveal that the BLYP/DNP level of theory performs remarkably well for predicting lignin degradation under pyrolysis reactions. Since we have gone beyond the dimers, we found a range of BDE values. Furthermore, the β-O-4′ homolytic cleavage reactions have been proposed to be barrierless, and as such, the activation energies can be approximated by the reaction energy. Thus, even a 1 kcal mol^{-1} difference in E_A will lead to factors difference in rate coefficients due to exponential dependence of the Arrhenius equation on E_A. This propagation of BDE range would affect kinetic (or reactor) modeling efforts of fast pyrolysis significantly where the purpose of the modeling efforts is aimed to control product selectivity and yield. Our systematic study on BDE of this large model oligomer is of practical significance, particularly to a broad readership including those interested in constructing detailed kinetic models and understanding the fundamental chemistry behind complex reacting systems involving fast pyrolysis of biomass to fuels.

■ ASSOCIATED CONTENT

Supporting Information

The Supporting Information is available free of charge at https://pubs.acs.org/doi/10.1021/acs.energyfuels.0c01573.

Variation of reaction enthalpies (BDE) along 9 pathways in primary pyrolysis temperature range; standard enthalpy of formation (ΔH°_f) for all species at reference temperature 298.15 K; heat capacity (C_p) and entropy (S) variation with temperature; electronic energy for all structures; Gibbs free energy (G) variation with temperature (PDF)

■ AUTHOR INFORMATION

Corresponding Author

Andrew J. Adamczyk − *Department of Chemical Engineering, Auburn University, Auburn, Alabama 36849, United States;* orcid.org/0000-0002-9523-7849; Email: aja0056@auburn.edu

Authors

Tanzina Azad − *Department of Chemical Engineering, Auburn University, Auburn, Alabama 36849, United States*

Jonathan D. Schuler − *Department of Chemical Engineering, Auburn University, Auburn, Alabama 36849, United States*

Maria L. Auad − *Department of Chemical Engineering and Center for Polymer and Advanced Composites, Auburn University, Auburn, Alabama 36849, United States;* orcid.org/0000-0001-6932-5645

Thomas Elder − *United States Department of Agriculture (USDA)-Forest Service, Southern Research Station, Auburn University, Auburn, Alabama 36849, United States;* orcid.org/0000-0003-3909-2152

Complete contact information is available at: https://pubs.acs.org/10.1021/acs.energyfuels.0c01573

Notes

The authors declare no competing financial interest.

■ ACKNOWLEDGMENTS

We are grateful for the support of this work by the Alabama Supercomputing Center, Auburn University Hopper high-performance compute cluster resources, USDA grant 18-JV-11330131-073 and Auburn University new faculty start-up funding.

■ REFERENCES

(1) Vanholme, R.; De Meester, B.; Ralph, J.; Boerjan, W. Lignin biosynthesis and its integration into metabolism. *Curr. Opin. Biotechnol.* **2019**, *56*, 230−239.

(2) Ralph, J.; Lundquist, K.; Brunow, G.; Lu, F.; Kim, H.; Schatz, P. F.; Marita, J. M.; Hatfield, R. D.; Ralph, S. A.; Christensen, J. H.; Boerjan, W. Lignins: Natural polymers from oxidative coupling of 4-hydroxyphenylpropanoids. *Phytochem. Rev.* **2004**, *3*, 29−60.

(3) Liu, Q. Q.; Luo, L.; Zheng, L. Q. Lignins: Biosynthesis and Biological Functions in Plants. *Int. J. Mol. Sci.* **2018**, *19*, No. 335.

(4) Bonawitz, N. D.; Chapple, C. The Genetics of Lignin Biosynthesis: Connecting Genotype to Phenotype. In *Annual Review of Genetics*; Campbell, A.; Lichten, M.; Schupbach, G., Eds.; Annual Reviews: Palo Alto, 2010; Vol. *44*, pp 337−363.

(5) Miao, Y. C.; Liu, C. J. ATP-binding cassette-like transporters are involved in the transport of lignin precursors across plasma and vacuolar membranes. *Proc. Natl. Acad. Sci. U.S.A.* **2010**, *107*, 22728−22733.

(6) Katahira, R.; Elder, T.; Beckham, G. T. A Brief Introduction to Lignin Structure. In *Lignin Valorization: Emerging Approaches*; The Royal Society of Chemistry, 2018.

(7) Higuchi, T. Biosynthesis of Lignin. In *Biosynthesis and Biodegradation of Wood Components*; Higuchi, T., Ed.; Academic Press, Inc, 1985; pp 141−160.

(8) Elder, T.; del Rio, J. C.; Ralph, J.; Rencoret, J.; Kim, H.; Beckham, G. T. Radical coupling reactions of piceatannol and monolignols: A density functional theory study. *Phytochemistry* **2019**, *164*, 12−23.

(9) Sederoff, R. R.; MacKay, J. J.; Ralph, J.; Hatfield, R. D. Unexpected variation in lignin. *Curr. Opin. Plant Biol.* **1999**, *2*, 145−152.

(10) Vanholme, R.; Morreel, K.; Ralph, J.; Boerjan, W. Lignin engineering. *Curr. Opin. Plant Biol.* **2008**, *11*, 278−285.

(11) Vanholme, R.; Morreel, K.; Darrah, C.; Oyarce, P.; Grabber, J. H.; Ralph, J.; Boerjan, W. Metabolic engineering of novel lignin in biomass crops. *New Phytol.* **2012**, *196*, 978−1000.

(12) Boerjan, W.; Ralph, J.; Baucher, M. Lignin biosynthesis. *Annu. Rev. Plant Biol.* **2003**, *54*, 519−546.

(13) Kawamoto, H.; Horigoshi, S.; Saka, S. Pyrolysis reactions of various lignin model dimers. *J. Wood Sci.* **2007**, *53*, 168−174.

(14) Dorrestijn, E.; Laarhoven, L. J. J.; Arends, I.; Mulder, P. The occurrence and reactivity of phenoxyl linkages in lignin and low rank coal. *J. Anal. Appl. Pyrolysis* **2000**, *54*, 153−192.

(15) Ralph, J.; Lapierre, C.; Boerjan, W. Lignin structure and its engineering. *Curr. Opin. Biotechnol.* **2019**, *56*, 240−249.

(16) Bridgwater, A. V.; Meier, D.; Radlein, D. An overview of fast pyrolysis of biomass. *Org. Geochem.* **1999**, *30*, 1479−1493.

(17) Mohan, D.; Pittman, C. U.; Steele, P. H. Pyrolysis of wood/biomass for bio-oil: A critical review. *Energy Fuels* **2006**, *20*, 848−889.

(18) Bridgwater, A. V. Review of fast pyrolysis of biomass and product upgrading. *Biomass Bioenergy* **2012**, *38*, 68−94.
(19) Zhu, H. L.; Luo, W.; Ciesielski, P. N.; Fang, Z. Q.; Zhu, J. Y.; Henriksson, G.; Himmel, M. E.; Hu, L. B. Wood-Derived Materials for Green Electronics, Biological Devices, and Energy Applications (vol 116, pg 9305, 2016). *Chem. Rev.* **2016**, *116*, 12650.
(20) Gonzalez-Quiroga, A.; Djokic, M. R.; Van Geem, K. M.; Marin, G. B. Conversion of Solid Waste to Diesel via Catalytic Pressureless Depolymerization: Pilot Scale Production and Detailed Compositional Characterization. *Energy Fuels* **2016**, *30*, 8292−8303.
(21) Barde, M.; Edmunds, C. W.; Labbe, N.; Auad, M. L. Fast pyrolysis bio-oil from lignocellulosic biomass for the development of bio-based cyanate esters and cross-linked networks. *High Perform. Polym.* **2019**, *31*, 1140−1152.
(22) Barde, M.; Avery, K.; Edrnunds, C. W.; Labbe, N.; Auad, M. L. Cross-Linked Acrylic Polymers from the Aqueous Phase of Biomass Pyrolysis Oil and Acrylated Epoxidized Soybean Oil. *ACS Sustainable Chem. Eng.* **2019**, *7*, 2216−2224.
(23) Hernández, B. S.; Barde, M.; Via, B.; Auad, M. L. Sustainable products from bio-oils. *MRS Bull.* **2017**, *42*, 365−370.
(24) Shen, D. K.; Jin, W.; Hu, J.; Xiao, R.; Luo, K. H. An overview on fast pyrolysis of the main constituents in lignocellulosic biomass to valued-added chemicals: Structures, pathways and interactions. *Renewable Sustainable Energy Rev.* **2015**, *51*, 761−774.
(25) Papari, S.; Hawboldt, K. A review on the pyrolysis of woody biomass to bio-oil: Focus on kinetic models. *Renewable Sustainable Energy Rev.* **2015**, *52*, 1580−1595.
(26) Mushrif, S. H.; Vasudevan, V.; Krishnamurthy, C. B.; Venkatesh, B. Multiscale molecular modeling can be an effective tool to aid the development of biomass conversion technology: A perspective. *Chem. Eng. Sci.* **2015**, *121*, 217−235.
(27) Asmadi, M.; Kawamoto, H.; Saka, S. The effects of combining guaiacol and syringol on their pyrolysis. *Holzforschung* **2012**, *66*, 323−330.
(28) Kawamoto, H.; Nakamura, T.; Saka, S. Pyrolytic cleavage mechanisms of lignin-ether linkages: A study on p-substituted dimers and trimers. *Holzforschung* **2008**, *62*, 50−56.
(29) Kawamoto, H.; Ryoritani, M.; Saka, S. Different pyrolytic cleavage mechanisms of β-ether bond depending on the side-chain structure of lignin dimers. *J. Anal. Appl. Pyrolysis* **2008**, *81*, 88−94.
(30) Britt, P. F.; Buchanan, A. C.; Cooney, M. J.; Martineau, D. R. Flash vacuum pyrolysis of methoxy-substituted lignin model compounds. *J. Org. Chem.* **2000**, *65*, 1376−1389.
(31) Britt, P. F.; Kidder, M. K.; Buchanan, A. C. Oxygen substituent effects in the pyrolysis of phenethyl phenyl ethers. *Energy Fuels* **2007**, *21*, 3102−3108.
(32) Holmelid, B.; Kleinert, M.; Barth, T. Reactivity and reaction pathways in thermochemical treatment of selected lignin-like model compounds under hydrogen rich conditions. *J. Anal. Appl. Pyrolysis* **2012**, *98*, 37−44.
(33) Banyasz, J. L.; Li, S.; Lyons-Hart, J.; Shafer, K. H. Gas evolution and the mechanism of cellulose pyrolysis. *Fuel* **2001**, *80*, 1757−1763.
(34) Piskorz, J.; Radlein, D.; Scott, D. S. On The Mechanism Of The Rapid Pyrolysis Of Cellulose. *J. Anal. Appl. Pyrolysis* **1986**, *9*, 121−137.
(35) Conesa, J. A.; Caballero, J. A.; Marcilla, A.; Font, R. Analysis of different kinetic models in the dynamic pyrolysis of cellulose. *Thermochim. Acta* **1995**, *254*, 175−192.
(36) Elder, T. Bond Dissociation Enthalpies of a Dibenzodioxocin Lignin Model Compound. *Energy Fuels* **2013**, *27*, 4785−4790.
(37) Elder, T. Bond Dissociation Enthalpies of a Pinoresinol Lignin Model Compound. *Energy Fuels* **2014**, *28*, 1175−1182.
(38) Elder, T.; Beste, A. Density Functional Theory Study of the Concerted Pyrolysis Mechanism for Lignin Models. *Energy Fuels* **2014**, *28*, 5229−5235.
(39) Huang, J. B.; Liu, C.; Jin, Q. J.; Tong, H.; Li, W. M.; Wu, D. Density functional theory study on bond dissociation enthalpies for lignin dimer model compounds. *J. Renewable Sustainable Energy* **2014**, *6*, No. 033116.
(40) Hu, Y. M.; Zuo, L.; Liu, J. Y.; Sun, J. Y.; Wu, S. B. Chemical Simulation and Quantum Chemical Calculation of Lignin Model Compounds. *BioResources* **2016**, *11*, 1044−1060.
(41) Parthasarathi, R.; Romero, R. A.; Redondo, A.; Gnanakaran, S. Theoretical Study of the Remarkably Diverse Linkages in Lignin. *J. Phys. Chem. Lett.* **2011**, *2*, 2660−2666.
(42) Kim, S.; Chmely, S. C.; Nimos, M. R.; Bomble, Y. J.; Foust, T. D.; Paton, R. S.; Beckham, G. T. Computational Study of Bond Dissociation Enthalpies for a Large Range of Native and Modified Lignins. *J. Phys. Chem. Lett.* **2011**, *2*, 2846−2852.
(43) Jarvis, M. W.; Daily, J. W.; Carstensen, H. H.; Dean, A. M.; Sharma, S.; Dayton, D. C.; Robichaud, D. J.; Nimlos, M. R. Direct Detection of Products from the Pyrolysis of 2-Phenethyl Phenyl Ether. *J. Phys. Chem. A* **2011**, *115*, 428−438.
(44) Kishimoto, T.; Uraki, Y.; Ubukata, M. Easy synthesis of beta-O-4 type lignin related polymers. *Org. Biomol. Chem.* **2005**, *3*, 1067−1073.
(45) Kishimoto, T.; Uraki, Y.; Ubukata, M. Chemical synthesis of beta-O-4 type artificial lignin. *Org. Biomol. Chem.* **2006**, *4*, 1343−1347.
(46) Kishimoto, T.; Uraki, Y.; Ubukata, M. Synthesis of beta-O-4-type artificial lignin polymers and their analysis by NMR spectroscopy. *Org. Biomol. Chem.* **2008**, *6*, 2982−2987.
(47) Uraki, Y.; Sugiyama, Y.; Koda, K.; Kubo, S.; Kishimoto, T.; Kadla, J. F. Thermal Mobility of beta-O-4-Type Artificial Lignin. *Biomacromolecules* **2012**, *13*, 867−872.
(48) Bízik, F.; Tvaroska, I.; Remko, M. Conformational analysis of ester and ether linkages in lignin-arabinoxylan complexes. *Carbohydr. Res.* **1994**, *261*, 91−102.
(49) Simon, J. P.; Eriksson, K. E. L. A molecular mechanics investigation of lignin structure. 1. Conformational analysis of 1-Phenyl-2-Phenoxy-1,3-Propanediol using MM3. *Holzforschung* **1995**, *49*, 429−438.
(50) Garver, T. M.; Maa, K. J.; Marat, K. Conformational analysis and 2D NMR assignment strategies for lignin model compounds. The structure of acetoguaiacyl-dehydro-diisoeugenol methyl ether. *Can. J. Chem.* **1996**, *74*, 173−184.
(51) Vermaas, J. V.; Petridis, L.; Qi, X. H.; Schulz, R.; Lindner, B.; Smith, J. C. Mechanism of lignin inhibition of enzymatic biomass deconstruction. *Biotechnol. Biofuels* **2015**, *8*, No. 217.
(52) Petridis, L.; Schulz, R.; Smith, J. C. Simulation Analysis of the Temperature Dependence of Lignin Structure and Dynamics. *J. Am. Chem. Soc.* **2011**, *133*, 20277−20287.
(53) Petridis, L.; Smith, J. C. A Molecular Mechanics Force Field for Lignin. *J. Comput. Chem.* **2009**, *30*, 457−467.
(54) Vermaas, J. V.; Petridis, L.; Ralph, J.; Crowley, M. F.; Beckham, G. T. Systematic parameterization of lignin for the CHARMM force field. *Green Chem.* **2019**, *21*, 109−122.
(55) Orella, M. J.; Gani, T. Z. H.; Vermaas, J. V.; Stone, M. L.; Anderson, E. M.; Beckham, G. T.; Brushett, F. R.; Roman-Leshkov, Y. Lignin-KMC: A Toolkit for Simulating Lignin Biosynthesis. *ACS Sustainable Chem. Eng.* **2019**, *7*, 18313−18322.
(56) Rappe, A. K.; Casewit, C. J.; Colwell, K. S.; Goddard, W. A.; Skiff, W. M. UFF, A Full Periodic-Table Force-Field For Molecular Mechanics And Molecular-Dynamics Simulations. *J. Am. Chem. Soc.* **1992**, *114*, 10024−10035.
(57) Cornell, W. D.; Cieplak, P.; Bayly, C. I.; Gould, I. R.; Merz, K. M.; Ferguson, D. M.; Spellmeyer, D. C.; Fox, T.; Caldwell, J. W.; Kollman, P. A. A second generation force field for the simulation of proteins, nucleic acids, and organic molecules (vol 117, pg 5179, 1995). *J. Am. Chem. Soc.* **1996**, *118*, 2309.
(58) Mackerell, A. D.; Wiorkiewiczkuczera, J.; Karplus, M. An All-Atom Empirical Energy Function For The Simulation of Nucleic acids. *J. Am. Chem. Soc.* **1995**, *117*, 11946−11975.
(59) Sun, H. COMPASS: An ab initio force-field optimized for condensed-phase applications - Overview with details on alkane and benzene compounds. *J. Phys. Chem. B* **1998**, *102*, 7338−7364.
(60) Metropolis, N.; Rosenbluth, A. W.; Rosenbluth, M. N.; Teller, A. H.; Teller, E. Equation of State Calculations by Fast Computing Machines. *J. Chem. Phys.* **1953**, *21*, 1087−1092.

https://dx.doi.org/10.1021/acs.energyfuels.0c01573
Energy Fuels XXXX, XXX, XXX−XXX

(61) Sun, H. COMPASS: An ab Initio Force-Field Optimized for Condensed-Phase ApplicationsOverview with Details on Alkane and Benzene Compounds. *J. Phys. Chem. B* **1998**, *102*, 7338−7364.
(62) Delley, B. An All-Electron Numerical Method for Solving the Local Density Functional for Polyatomic Molecules. *J. Chem. Phys.* **1990**, *92*, 508−517.
(63) Delley, B. From molecules to solids with the DMol(3) approach. *J. Chem. Phys.* **2000**, *113*, 7756−7764.
(64) Perdew, J. P.; Burke, K.; Ernzerhof, M. Generalized gradient approximation made simple (vol 77, pg 3865, 1996). *Phys. Rev. Lett.* **1997**, *78*, 1396.
(65) Becke, A. D. Density-Functional Thermochemistry. 3. The Role of Exact Exchange. *J. Chem. Phys.* **1993**, *98*, 5648−5652.
(66) Tkatchenko, A.; Scheffler, M. Accurate Molecular Van Der Waals Interactions from Ground-State Electron Density and Free-Atom Reference Data. *Phys. Rev. Lett.* **2009**, *102*, No. 073005.
(67) Adamczyk, A. J.; Broadbelt, L. J. Thermochemical Property Estimation of Hydrogenated Silicon Clusters. *J. Phys. Chem. A* **2011**, *115*, 8969−8982.
(68) Adamczyk, A. J.; Broadbelt, L. J. The Role of Multifunctional Kinetics during Early-Stage Silicon Hydride Pyrolysis: Reactivity of Si2H2 Isomers with SiH4 and Si2H6. *J. Phys. Chem. A* **2011**, *115*, 2409−2422.
(69) Adamczyk, A. J.; Reyniers, M. F.; Marin, G. B.; Broadbelt, L. J. Exploring 1,2-Hydrogen Shift in Silicon Nanoparticles: Reaction Kinetics from Quantum Chemical Calculations and Derivation of Transition State Group Additivity Database. *J. Phys. Chem. A* **2009**, *113*, 10933−10946.
(70) Adamczyk, A. J.; Reyniers, M. F.; Marin, G. B.; Broadbelt, L. J. Kinetics of Substituted Silylene Addition and Elimination in Silicon Nanocluster Growth Captured by Group Additivity. *ChemPhysChem* **2010**, *11*, 1978−1994.
(71) Adamczyk, A. J.; Reyniers, M. F.; Marin, G. B.; Broadbelt, L. J. Kinetic correlations for H-2 addition and elimination reaction mechanisms during silicon hydride pyrolysis. *Phys. Chem. Chem. Phys.* **2010**, *12*, 12676−12696.
(72) Adamczyk, A. J.; Reyniers, M. F.; Marin, G. B.; Broadbelt, L. J. Hydrogenated amorphous silicon nanostructures: novel structure-reactivity relationships for cyclization and ring opening in the gas phase. *Theor. Chem. Acc.* **2011**, *128*, 91−113.
(73) Deng, S. D.; Du, G. B.; Li, X. H.; Xie, X. G. Performance, Reaction Mechanism, and Characterization of Glyoxal-Monomethylol Urea (G-MMU) Resin. *Ind. Eng. Chem. Res.* **2014**, *53*, 5421−5431.
(74) Tan, B. S.; Peng, R. F.; Li, H. B.; Jin, B.; Chu, S. J.; Long, X. P. Theoretical Investigation of an Energetic Fullerene Derivative. *J. Comput. Chem.* **2010**, *31*, 2233−2237.
(75) Wang, J. Q.; Liu, L. L.; Wilson, A. K. Oxidative Cleavage of the beta-O-4 Linkage of Lignin by Transition Metals: Catalytic Properties and the Performance of Density Functionals. *J. Phys. Chem. A* **2016**, *120*, 737−746.
(76) van Mourik, T.; Danilov, V. I.; Dailidonis, V. V.; Kurita, N.; Wakabayashi, H.; Tsukamoto, T. A DFT study of uracil and 5-bromouracil in nanodroplets. *Theor. Chem. Acc.* **2010**, *125*, 233−244.
(77) McQuarrie, D. A. *Statistical Mechanics*; Harper & Row, 1973.
(78) Van Speybroeck, V.; Marin, G. B.; Waroquier, M. Hydrocarbon bond dissociation enthalpies: From substituted aromatics to poly-aromatics. *ChemPhysChem* **2006**, *7*, 2205−2214.
(79) Wang, H. J.; Zhao, Y.; Wang, C.; Fu, Y.; Guo, Q. X. Theoretical Study on the Pyrolysis Process of Lignin Dimer Model Compounds. *Acta Chim. Sin.* **2009**, *67*, 893−900.
(80) Zhang, J. J.; Jiang, X. Y.; Ye, X. N.; Chen, L.; Lu, Q.; Wang, X. H.; Dong, C. Q. Pyrolysis mechanism of a beta-O-4 type lignin dimer model compound. *J. Therm. Anal. Calorim.* **2016**, *123*, 501−510.
(81) Kim, S.; Nimlos, M. R.; Bomble, Y. J.; Foust, T. D.; Paton, R. S.; Beckham, G. T.; Chmely, S. C. Computational Study of Bond Dissociation Enthalpies for a Large Range of Native and Modified Lignins. *J. Phys. Chem. Lett.* **2011**, *2*, 2846−2852.
(82) Lewars, E. G. Introduction to the Theory and Applications of Molecular and Quantum Mechanics. In *Computational Chemistry*, 2nd ed.; Springer, 2011.
(83) Younker, J. M.; Beste, A.; Buchanan, A. C. Computational study of bond dissociation enthalpies for lignin model compounds: beta-5 Arylcoumaran. *Chem. Phys. Lett.* **2012**, *545*, 100−106.
(84) Gonzalez-Quiroga, A.; Van Geem, K. M.; Marin, G. B. Towards first-principles based kinetic modeling of biomass fast pyrolysis. *Biomass Convers. Biorefin.* **2017**, *7*, 305−317.
(85) Voitkevich, O.; Kabo, G.; Blokhin, A.; Paulechka, Y.; Shishonok, M. Thermodynamic Properties of Plant Biomass Components. Heat Capacity, Combustion Energy, and Gasification Equilibria of Lignin. *J. Chem. Eng. Data* **2012**, *57*, 1903−1909.
(86) Hatakeyama, T.; Nakamura, K.; Hatakeyama, H. Studies On Heat-Capacity Of Cellulose And Lignin By Differential Scanning Calorimetry. *Polymer* **1982**, *23*, 1801−1804.

https://dx.doi.org/10.1021/acs.energyfuels.0c01573
Energy Fuels XXXX, XXX, XXX−XXX